Spin-wave multiple excitations in nanoscale classical Heisenberg antiferromagnets

Zhuofei Hou* and D. P. Landau†
Center for Simulational Physics, University of Georgia, Athens, Georgia 30602-2451, USA

G. M. Stocks‡
Center for Defect Physics, Oak Ridge National Laboratory, Oak Ridge, Tennessee 37831-6114, USA

G. Brown§
Department of Physics, The Florida State University, Tallahassee, Florida 32306-4350, USA

(Received 31 March 2014; revised manuscript received 1 February 2015; published 17 February 2015)

Monte Carlo and spin dynamics techniques have been used to perform large-scale simulations of the dynamic behavior of a nanoscale, classical, Heisenberg antiferromagnet on a simple-cubic lattice with linear sizes $L \leq 40$ at a temperature below the Néel temperature. Nanoparticles are modeled with completely free boundary conditions, i.e., six free surfaces, and nanofilms are modeled with two free surfaces in the spatial z direction and periodic boundaries parallel to the surfaces in the xy direction, which are compared to the "infinite" system with periodic boundary conditions. The temporal evolutions of spin configurations were determined numerically from coupled equations of motion for individual spins using a fast spin dynamics algorithm with the fourth-order Suzuki-Trotter decomposition of exponential operators, with initial spin configurations generated by Monte Carlo simulations. The local dynamic structure factor $S(q,\omega)$ was calculated from the local space- and time-displaced spin-spin correlation function. Multiple excitation peaks for wave vectors within the first Brillouin zone appear in the spin-wave spectra of the transverse component of dynamic structure factor $S^T(q,\omega)$ in the nanoscale classical Heisenberg antiferromagnet, which are lacking if periodic boundary conditions are used. With the assumption of q-space spin-wave reflections with broken momentum conservation due to free-surface confinements, we successfully explained those spectra quantitatively in the linear dispersion region. Meanwhile, we also observed two unexpected quantized spin-wave excitation modes in the spatial z direction in nanofilms for $S^T(q,\omega)$ not expected in bulk systems. The results of this study indicate the presence of unexpected forms of spin-wave excitation behavior that have yet to be observed experimentally but could be directly tested through neutron scattering experiments on nanoscale $RbMnF_3$ particles or films.

DOI: 10.1103/PhysRevB.91.064417 PACS number(s): 75.10.Hk, 75.40.Gb, 75.40.Mg

I. INTRODUCTION

The deterministic time-dependent dynamic behavior of "infinite" magnetic systems with periodic boundary conditions has been studied extensively via experiments [1–3] and spin dynamics simulations [4–9] with classical Heisenberg models. Early simulations for the transverse component of the dynamic structure factor, $S^T(q,\omega)$, on isotropic antiferromagnetic body-centered-cubic systems at temperatures below the critical temperature T_c, show a single spin-wave excitation peak of finite intensity with finite width, becoming narrow and increasing in excitation energy frequency ω as T decreases, which approaches the predictions of linear spin-wave theory, and a diffusive central peak increasing in strength with increasing T at $\omega = 0$. Both are in qualitative agreement with the experiments [2,3]. Large-scale computer simulations carried out by Tsai, Bunker, and Landau [6] on antiferromagnetic, isotropic, simple-cubic systems below T_c found that by fitting the line shape of $S^T(q,\omega)$ to a Lorentzian form [10], in the [100] direction the dispersion curves that result are approximately linear in wave vector for small q within the first Brillouin zone. For increasing T toward T_c the dispersion curve turns into a power law, reflecting the crossover from hydrodynamics to critical behavior with the dynamic critical exponent estimated to be $z = 1.43(0.03)$. This value is in agreement with the experimental estimate of the dynamic critical exponent $z = 1.43(0.04)$ [3]. With larger systems, Tsai and Landau [8] carried simulations to better probe the asymptotic critical region in momentum, and they estimated $z = 1.49(0.03)$ in good agreement with the renormalization-group theory and dynamic scaling predicted value [11–14] of $z = 1.5$ for an isotropic three-dimensional Heisenberg antiferromagnet. The dynamic behavior of the longitudinal component of the dynamic structure factor, $S^L(q,\omega)$, has been studied by Bunker and Landau [15]. For both the isotropic and anisotropic antiferromagnets, both annihilation and creation two-spin-wave peaks are observed. The splitting of the longitudinal spin-wave peak into two spin-wave peaks with the energy separation of twice the energy gap at the Brillouin zone center is predicted for all anisotropic antiferromagnets.

Recent developments in the field of magnetic material applications brought much attention to the static and dynamic properties of confined magnetic elements of small dimensions [16]. Recent experiments [17–19] on micron-scale array elements showed quantized and localized spin-wave excitation modes as eigenexcitations by the selection rules introduced by lateral confined boundary conditions of the elements. In

*zhuofei@physast.uga.edu
†dlandau@physast.uga.edu
‡stocksgm@ornl.gov
§gbrown@fsu.edu

addition, the intrinsic broken translational invariance caused by confinement effects in one or more directions in those small laterally confined magnetic elements leads to the broken conservation law of the corresponding momentum for a spin wave, which brings uncertainty into the wave vector for a specific spin-wave excitation energy. This uncertainty is reported to be inversely proportional to the confinement length [20]. Therefore, instead of a continuous spin-wave spectrum with spin-wave excitation energy frequency uniquely determined by each wave vector, quantized spin-wave excitation modes, each of them observed within a given wave-vector interval, are obtained from those experiments.

Extensive Monte Carlo simulations for nanoscale magnetic systems have been performed by Brown *et al.* [21,22] on the study of thermoinduced magnetization (TiM), which is predicted to lead to ferromagnetic properties in antiferromagnetic nanoparticles below the Néel temperature T_N. The Monte Carlo estimates for the magnetization and susceptibility indicate that TiM is an intrinsic property of the antiferromagnetic Heisenberg model below the T_N, but they do not tell us anything about the dynamic behavior.

The work presented here followed the previous work done by Brown *et al.* [21,22]. To gain further understanding of the dynamic properties of nanoscale antiferromagnetic systems, we carried out large-scale spin dynamics simulations of the dynamic behavior of the nanoscale classical Heisenberg antiferromagnet on a simple-cubic lattice. This study is not restricted to the nanoscale antiferromagnetic case, i.e., it can also be extended to ferromagnetic systems. We focus mainly on the spin-wave excitation spectra of the transverse component of the dynamic structure factor $S^T(q,\omega)$ confined in the nanoscale isotropic classical Heisenberg antiferromagnets at a temperature below the Néel temperature. Section II of this paper contains the definition of the model and introduces the simulation background. In Sec. III we present and discuss our simulation results, and a summary is given in Sec. IV.

II. MODEL AND METHODS

A. Model

We propose to study the spin dynamics of antiferromagnetic nanoparticles and nanofilms with spin interactions described by a classical Heisenberg Hamiltonian of the form

$$\mathcal{H} = -J_{\mathrm{AF}} \sum_{\langle \mathbf{r},\mathbf{r}' \rangle} \mathbf{S}_{\mathbf{r}} \cdot \mathbf{S}_{\mathbf{r}'}, \tag{1}$$

where $\mathbf{S}_{\mathbf{r}}$ is a three-dimensional classical spin of unit length at site $\mathbf{r}$, and $\langle \mathbf{r},\mathbf{r}' \rangle$ denotes nearest-neighbor pairs of spins. $J_{\mathrm{AF}} < 0$ is the antiferromagnetic nearest-neighbor exchange interaction between $\mathbf{S}_{\mathbf{r}}$ and $\mathbf{S}_{\mathbf{r}'}$.

The model nanoparticles consist of L^3 spins on an $L \times L \times L$ simple-cubic lattice with completely free boundary conditions with six free surfaces. Our model nanofilms consist of $L_{xy}^2 L_z$ spins on an $L_{xy} \times L_{xy} \times L_z$ simple-cubic lattice with partially free boundary conditions with two free surfaces in the spatial z direction and periodic boundaries parallel to the surfaces in the xy direction. L_{xy} and L_z are the linear dimensions in the xy and z directions, respectively.

B. Local dynamic structure factor $S(\mathbf{r}_0,\mathbf{q},\omega)$

Fully periodic boundary conditions have been implemented to preserve the translational invariance and emulate "infinite" systems. In the modeling of nanofilms and nanoparticles in this work, we introduced free boundary conditions either partially in one spatial direction or completely in all spatial directions. As one of the consequences of introducing free boundary conditions, the translational invariance of the system is broken in the directions in which we introduced free boundary conditions. Accordingly, to express the broken translational symmetry, the formalism of the space- and time-displaced spin-spin correlation function has been modified from a translational invariant one with a form of $C(\mathbf{r},t)$ to a localized one with a form of $C(\mathbf{r}_0,\mathbf{r},t)$, where the parameter $\mathbf{r}_0$ denotes a fixed lattice site as the starting point for the calculation of the local correlation. Based on the specific localization performed, $\mathbf{r}_0$ can be chosen to be fixed at the bulk center or the surface center of nanofilms and nanoparticles, or even the lattice corner of nanoparticles, i.e., $\mathbf{r}_0 \Rightarrow$ bulk center, surface center, or lattice corner.

The definition of the local space- and time-displaced spin-spin correlation function is defined as

$$C^k(\mathbf{r}_0,\mathbf{r},t) = \langle S^k(\mathbf{r}_0,t_0) S^k(\mathbf{r}_0+\mathbf{r},t_0+t)\rangle - \langle S^k(\mathbf{r}_0,t_0)\rangle \langle S^k(\mathbf{r}_0+\mathbf{r},t_0+t)\rangle, \tag{2}$$

where $\mathbf{r}_0$ and t_0 denote the spatial and temporal starting points for the local correlation function, respectively; $\mathbf{r}$ and t denote the spatial and time intervals, respectively; $\langle \cdots \rangle$ gives the ensemble average; $k = x$, y or z; $S^k(\mathbf{r}_0+\mathbf{r},t_0+t)$ stands for the k component of a spin at the lattice site $\mathbf{r}+\mathbf{r}_0$ and the time t_0+t. The displacement $\mathbf{r}$ is in units of the lattice unit cell length a. In the case of antiferromagnets, the wave vectors are measured with respect to the (π,π,π) point, which corresponds to the Brillouin zone center.

The local dynamic structure factor $S(\mathbf{r}_0,\mathbf{q},\omega)$ is the Fourier transform of the local space- and time-displaced spin-spin correlation function $C(\mathbf{r}_0,\mathbf{r},t)$, as given by

$$S^k(\mathbf{r}_0,\mathbf{q},\omega) = \frac{1}{N_{\mathrm{spin}}} \sum_{\mathbf{r}} e^{i\mathbf{q}\cdot\mathbf{r}} \times \int_{-\infty}^{+\infty} e^{-i\omega t} C^k(\mathbf{r}_0,\mathbf{r},t) \frac{dt}{\sqrt{2\pi}}, \tag{3}$$

where $k = x$, y, or z; N_{spin} is the total number of spins in a lattice.

The calculation of the local correlation is performed in the [100] direction, i.e., in momentum space $\mathbf{q} = (q,0,0)$. q is determined for $\mathbf{r}_0 \Rightarrow$bulk center as

$$q = \begin{cases} \frac{2\pi n_q}{L}, & n_q = 0,1,2,\ldots, \quad n_{q_{\max}} \equiv \frac{L}{2} \quad \text{for even } L, \\ \frac{2\pi n_q}{L}, & n_q = 0,1,2,\ldots, \quad n_{q_{\max}} \equiv \frac{L-1}{2} \quad \text{for odd } L. \end{cases} \tag{4}$$

C. Simulation background

The Heisenberg model has true dynamics with the real-time evolution of spins governed by the coupled equations of

motion [23],

$$\frac{d}{dt}\mathbf{S_r} = \frac{\partial \mathcal{H}}{\partial \mathbf{S_r}} \times \mathbf{S_r}, \tag{5}$$

which can be rewritten as

$$\frac{d}{dt}\mathbf{S_r} = \mathbf{H_{eff\,r}} \times \mathbf{S_r}, \tag{6}$$

where $\mathbf{H_{eff\,r}}$ is the effective field at site $\mathbf{r}$, given by

$$H^k_{\mathbf{eff\,r}} = -J_{\mathrm{AF}} \sum_{\langle \mathbf{r},\mathbf{r'}\rangle} S^k_{\mathbf{r'}}, \qquad k = x, y, z, \tag{7}$$

where the sum is performed over all nearest-neighbor sites of $\mathbf{r}$. If we denote $\mathbf{S_r}$ as

$$\mathbf{S_r} = \begin{pmatrix} S^x_{\mathbf{r}} \\ S^y_{\mathbf{r}} \\ S^z_{\mathbf{r}} \end{pmatrix}, \tag{8}$$

Eq. (6) can be rewritten as

$$\frac{d}{dt}\mathbf{S_r} = \begin{bmatrix} 0 & -H^z_{\mathbf{eff\,r}} & H^y_{\mathbf{eff\,r}} \\ H^z_{\mathbf{eff\,r}} & 0 & -H^x_{\mathbf{eff\,r}} \\ -H^y_{\mathbf{eff\,r}} & H^x_{\mathbf{eff\,r}} & 0 \end{bmatrix} \mathbf{S_r} \equiv R\mathbf{S_r}, \tag{9}$$

for which the formal solution is

$$\mathbf{S_r}(t+\Delta) = e^{R\Delta}\mathbf{S_r}(t), \tag{10}$$

where Δ is the time step for the integration of the equations of motion.

The general recipe of spin dynamics is to generate N equilibrium spin configurations drawn from a canonical ensemble at a specific temperature T using a hybrid Monte Carlo (MC) method, and to use these N equilibrium spin configurations as starting states for the integration of the coupled equations of motion using the spin dynamics (SD) method, with the real SD time evolving from $t = 0$ to $t_{\max} = n_t dt$, where n_t is the total number of SD time steps and dt is the SD time step [24]. From those data, $C(\mathbf{r}_0,\mathbf{r},t)$ is calculated for time displacement t, ranging from 0 to a cutoff time $t_{\mathrm{cutoff}} = n_{\mathrm{cutoff}} dt$, where n_{cutoff} is the number of SD time steps for cutoff time displacement. We take a set of N initial conditions for a fixed lattice size and average their results for $C(\mathbf{r}_0,\mathbf{r},t)$. If this set of N configurations is an equilibrium distribution at the temperature T, then the average over all the $C(\mathbf{r}_0,\mathbf{r},t)$ will be a result for the local space-time correlation function at T for a finite lattice size.

We simulated the behavior of the simple-cubic classical Heisenberg antiferromagnetic nanostructures with linear dimension less than 40 at a specific temperature $T = 0.4T_N$, where T_N has been determined to a high degree of accuracy of $T_N = 1.442\,929(77)|J|/k_B$, by Chen *et al.* [4] for the isotropic Heisenberg system with simple-cubic lattice geometry. We used the hybrid MC method, in which for isotropic systems a single hybrid MC step consists of two METROPOLIS steps and eight overrelaxation steps [25,26] to generate an N equilibrium distribution of states at $T = 0.4T_N$. Typically, 5000 hybrid MC steps were used to generate each equilibrium configuration, and the coupled equations of motion were then integrated numerically using these states as initial spin configurations. For nanofilms with the same $L_{xy} = 20$, the total number of equilibrium configurations generated by the hybrid MC is $N = 4000$ for $L_z = 10$; $N = 1500$ for $L_z = 20$; $N = 1500$ for $L_z = 30$. For nanofilms with the same $L_z = 10$, $N = 5000$ for $L_{xy} = 10$; $N = 4000$ for $L_{xy} = 20$; $N = 2600$ for $L_{xy} = 30$. For nanoparticles, $N = 5000$ for $L = 10$; $N = 5000$ for $L = 14$; $N = 4000$ for $L = 20$.

The coupled equations of motion were integrated using an algorithm based on the fourth-order Suzuki-Trotter decomposition of the exponential operator, by which the magnetization will be conserved up to terms of the order $(dt)^4$ (global truncation error) [27,28]. Typically, numerical integrations were performed to a maximum time $t_{\max} = 1000/|J|$ with $n_t = 5000$ and SD time step $dt = 0.2/|J|$. $t_{\mathrm{cutoff}} = 800/|J|$ with $n_{\mathrm{cutoff}} = 4000$ was used as the cutoff time for the calculation of $C(\mathbf{r}_0,\mathbf{r},t)$.

In our simulations for antiferromagnetic nanostructures, we applied component-regrouping on the local dynamic structure factor in the spin space into a longitudinal component, which is parallel to the order parameter of the system, i.e., the staggered magnetization, as

$$S^L(\mathbf{r}_0,\mathbf{q},\omega) = S^z(\mathbf{r}_0,\mathbf{q},\omega), \tag{11}$$

and a transverse component, which is perpendicular to the order parameter of the system, as

$$S^T(\mathbf{r}_0,\mathbf{q},\omega) = \tfrac{1}{2}[S^x(\mathbf{r}_0,\mathbf{q},\omega) + S^y(\mathbf{r}_0,\mathbf{q},\omega)]. \tag{12}$$

For an antiferromagnet, the order parameter, i.e., the staggered magnetization, is not a constant of motion; therefore, regrouping components of the spin parallel (longitudinal component) and perpendicular (transverse component) to the order parameter is challenging. As we integrate the equations of motion, the direction of the staggered magnetization changes slightly because it is not a conserved quantity. Our approach to overcome this problem is to rotate the coordinate frame of reference continually after each integration step so that the z axis is to be realigned to the staggered magnetization and restored as the longitudinal direction.

III. RESULTS

A. Spectra for $S^T(\mathbf{r_0},\mathbf{q},\omega)$ for isotropic antiferromagnetic nanofilms

In this section, we give the results for the transverse component of the local dynamic structure factor $S^T(\mathbf{r}_0,\mathbf{q},\omega)$ with $\mathbf{r}_0 \Rightarrow$ bulk center for isotropic, antiferromagnetic nanofilms on an $L_{xy} \times L_{xy} \times L_z$ simple-cubic lattice. The results were obtained in the periodic boundary directions, denoted as the *PBCXY* [100] directions, parallel to the free surfaces, as shown in Fig. 1.

Figure 2 shows the spectra for $S^T(\mathbf{r}_0,\mathbf{q},\omega)$ with the same $L_{xy} = 20$ and three different thicknesses, i.e., $L_z = 10$, 20, and 30. For convenience, we labeled the y axis of our results with $S^T(\mathbf{r}_0,n_q,\omega)$ with $n_q = 0,1,2,\ldots$. In the figure, we give the spectra for $n_q = 0,1,2,\ldots,5$.

The vertical dashed lines in the figure labeled with ω_{PBC} show the single spin-wave excitation locations for each wave vector of the "infinite" system with periodic boundary

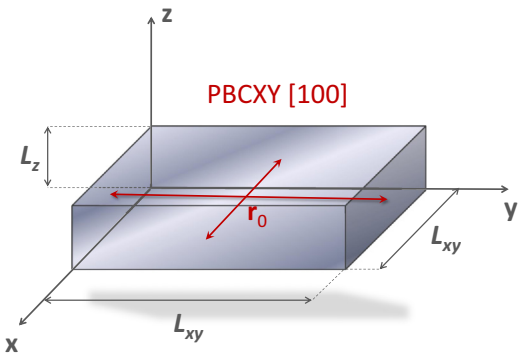

FIG. 1. (Color online) *PBCXY* [100] directions with $\mathbf{r}_0 \Rightarrow$ bulk center for isotropic, antiferromagnetic nanofilms.

conditions. Two major observations can be made pertinent to the above spectra:

(i) Multiple excitation peaks for wave vectors within the first Brillouin zone appear in the spin-wave spectra for the transverse component of the local dynamic structure factor $S^T(\mathbf{r}_0,n_q,\omega)$ in the classical Heisenberg isotropic antiferromagnetic nanofilms, which are lacking if periodic boundary conditions are used.

(ii) Negative spin-wave excitation peaks originating from the negative local correlation between opposite sublattices of antiferromagnetic systems were observed in spectra for each wave vector.

In addition to the above two major observations, we also observed that, as the thickness L_z of nanofilms, i.e., the distance between the free surfaces, becomes larger, the main excitation peak for some wave vectors, e.g., $n_q = 1,2,3$, shifts closer to ω_{PBC}. This observation is reasonable considering the

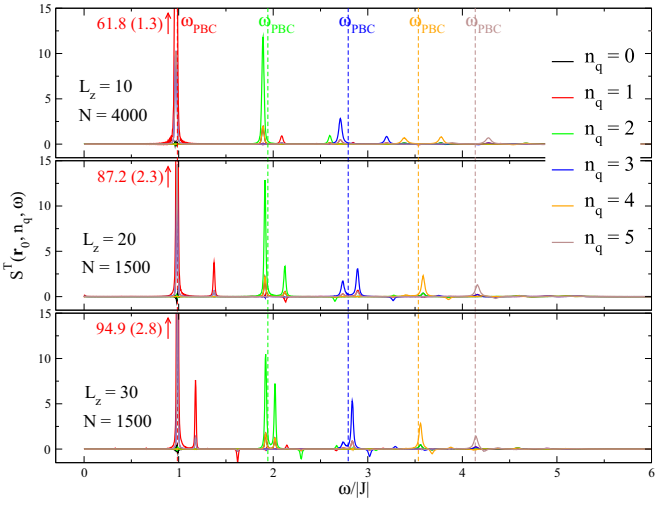

FIG. 2. (Color online) The spectra for $S^T(\mathbf{r}_0,\mathbf{q},\omega)$ obtained from isotropic, antiferromagnetic nanofilms with the same $L_{xy} = 20$ and three different thicknesses, i.e., $L_z = 10$, 20, and 30. The results were obtained in the *PBCXY* [100] directions, i.e., the directions parallel to the free surfaces, with $\mathbf{r}_0 \Rightarrow$ bulk center at $T = 0.4T_N$ with SD parameters of $n_t = 5000$, $n_{\text{cutoff}} = 4000$, and $dt = 0.2/|J|$. We give the spectra for $n_q = 0,1,2,\ldots,5$. N is the total number of initial configurations.

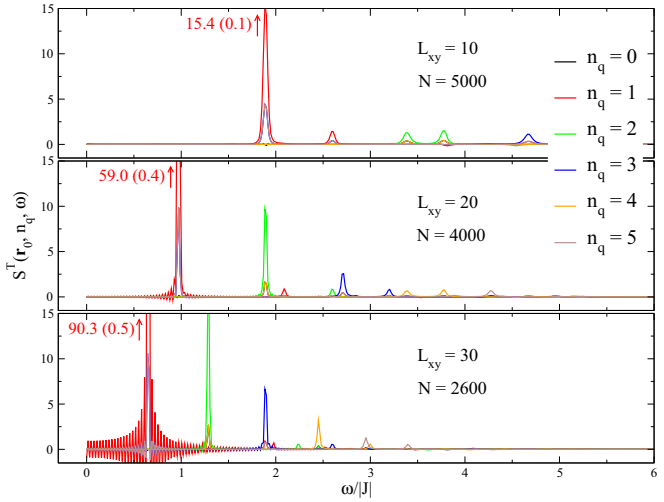

FIG. 3. (Color online) The spectra for $S^T(\mathbf{r}_0,\mathbf{q},\omega)$ obtained from isotropic, antiferromagnetic nanofilms with the same $L_z = 10$ and three different horizontal dimensions, i.e., $L_{xy} = 10$, 20, and 30. The results were obtained in the *PBCXY* [100] directions, i.e., the directions parallel to the free surfaces, with $\mathbf{r}_0 \Rightarrow$ bulk center at $T = 0.4T_N$ with SD parameters of $n_t = 5000$, $n_{\text{cutoff}} = 4000$, and $dt = 0.2/|J|$. We give the spectra for $n_q = 0,1,2,\ldots,5$. N is the total number of initial configurations.

free-surface effects become weaker as the separation between free surfaces increases, and thus the dynamics behaves more like that of the "infinite" system with periodic boundary conditions.

To complete our results, in Fig. 3 we present a further set of spectra $S^T(\mathbf{r}_0,\mathbf{q},\omega)$ for nanofilms having the same thickness $L_z = 10$ but with three different horizontal dimensions, i.e., $L_{xy} = 10$, 20, and 30. Note that we did independent runs with the identical dimension parameters for the nanofilm shown in the top panel of Fig. 2 and that in the middle panel of Fig. 3, i.e., both are $L_{xy} = 20$ and $L_z = 10$, which gave consistent results within error bars. The larger oscillations in Fig. 3 are due to larger finite-time cutoff used in the Fourier transform of the local correlation function.

The spectra in Fig. 3 are very similar to those of Fig. 2. It should be noted that the bigger oscillations of the spectra for $n_q = 1$ in Fig. 3 for $L_{xy} = 20$ and 30 are due to the finite-time cutoff n_{cutoff}, which introduces oscillations into the results of the Fourier transformation. These oscillations, however, can be smoothed out by convoluting the local correlation function with a Gaussian resolution function $e^{-\frac{1}{2}t\delta_\omega}$ in the time Fourier transformation, where δ_ω is a parameter determining the resolution in frequency and needs to be chosen properly such that effects of the cutoff in the evolution time can be neglected [4]. The shifting to the lower energy frequency of the main excitation peak in Fig. 3 is due to the finite-size effects in the xy directions with periodic boundary conditions.

The most significant observation of the spectra for $S^T(\mathbf{r}_0,n_q,\omega)$ in isotropic, antiferromagnetic nanofilms (Figs. 2 and 3) is the multiple spin-wave excitation peaks with the intensity decreasing with increasing energy. Given that the intensity of these peaks decreases so significantly with increasing energy, it is important to demonstrate that they

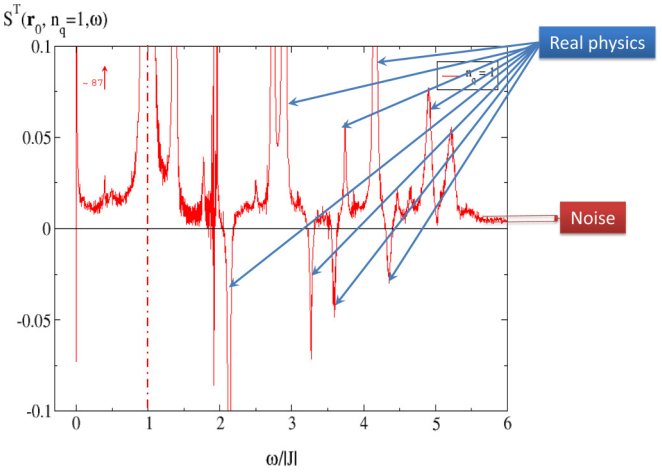

FIG. 4. (Color online) High-resolution plot of the raw simulation data of multiple spin-wave excitation peaks illustrating the differences in the magnitude of the multiple spin-wave peaks and the intrinsic noise in our simulations for $n_q = 1$ of the nanofilm with $L_{xy} = L_z = 20$. Note that the noise is $\sim 10^{-4}$ as big as the single spin-wave peak.

correspond to real excitations rather than the statistical noise inherent in the simulations. Figure 4 shows the comparison between the magnitude of those multiple spin-wave peaks and the magnitude of the intrinsic noise in our simulations for $n_q = 1$ of the nanofilm with $L_{xy} = L_z = 20$. As shown in the figure, there is a significant difference in the magnitude, which indicates that those multiple spin-wave excitations do not originate from noise fluctuations. Note that the noise is $\sim 10^{-4}$ as big as the single spin-wave peak.

B. q-space spin-wave reflection: Quantitative explanation of multiple spin-wave excitations in the spectra for $S^T(\mathbf{r}_0, \mathbf{q}, \omega)$ for isotropic antiferromagnetic nanofilms

As mentioned in Sec. I, for small laterally confined magnetic systems such as nanofilms or nanoparticles, there is intrinsic broken translational invariance caused by free-surface confinement effects in one or more directions, which leads to a broken conservation law of the corresponding spin-wave momentum. The broken conservation law of momentum brings uncertainty into the wave vector for a specific spin-wave excitation energy. To explain the multiple spin-wave excitation peaks, we proposed the assumption of q-space spin-wave reflection with broken momentum conservation. That is, in the linear dispersion region with small momentum q, the reflected spin-wave energy and momentum should satisfy a geometric relationship defined by

$$\frac{\omega_{\text{refl}}}{\omega_{\text{bulk}}} = \frac{q_{\text{refl}}}{q_{\text{bulk}}}, \tag{13}$$

where q_{bulk} and q_{refl} are the bulk momentum and reflected momentum, respectively; ω_{bulk} and ω_{refl} are the bulk energy frequency and reflected energy frequency, respectively. Figure 5 gives an illustration of this assumption.

With the assumption of q-space spin-wave reflection with broken momentum conservation, we successfully explained the multiple spin-wave excitation spectra quantitatively in the

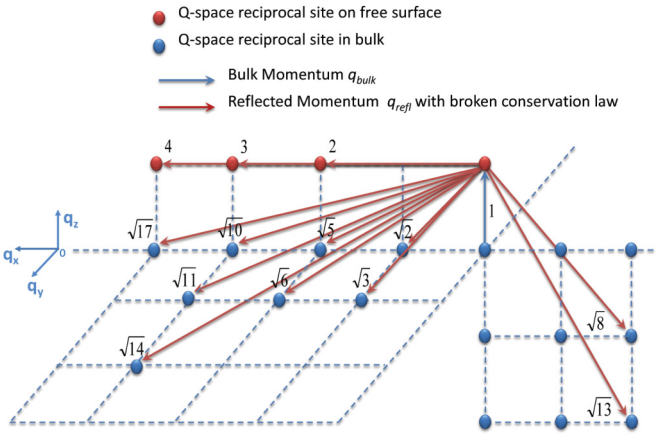

FIG. 5. (Color online) An illustration of the assumption of q-space spin-wave reflection with broken momentum conservation.

linear dispersion region with small momentum q. Figure 6 gives the same spectra shown in Fig. 4. The thick red dashed line gives the single spin-wave excitation location for the wave vector of $n_q = 1$ of the system with periodic boundary conditions; the thick black dashed line labeled with $\omega = \omega_{\text{bulk}}$ gives the bulk excitation location for the wave vector of $n_q = 1$

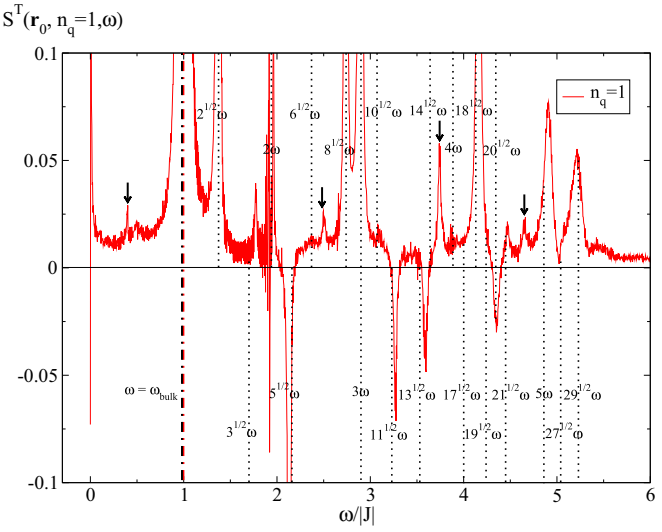

FIG. 6. (Color online) Determination of multiple spin-wave excitation locations with the assumption of q-space spin-wave reflection with broken momentum conservation in the linear dispersion region with small momentum of $n_q = 1$ for an isotropic, antiferromagnetic nanofilm with a lattice size of $L_{xy} = L_z = 20$. The results were obtained in the *PBCXY* [100] directions, i.e., the directions parallel to the free surfaces, with $\mathbf{r}_0 \Rightarrow$ bulk center at $T = 0.4T_N$ with SD parameters of $n_t = 5000$, $n_{\text{cutoff}} = 4000$, and $dt = 0.2/|J|$. The thick red dashed line gives the single spin-wave excitation location for the wave vector of $n_q = 1$ of the system with periodic boundary conditions; the thick black dashed line labeled with $\omega = \omega_{\text{bulk}}$ gives the bulk excitation location for the wave vector of $n_q = 1$ of the nanofilm; the thick black downward arrows labeled in the figure give the locations of excitation peaks disturbed by the unexpected excitation modes in *FBCZ* [100] perpendicular directions that will be discussed in Sec. III E.

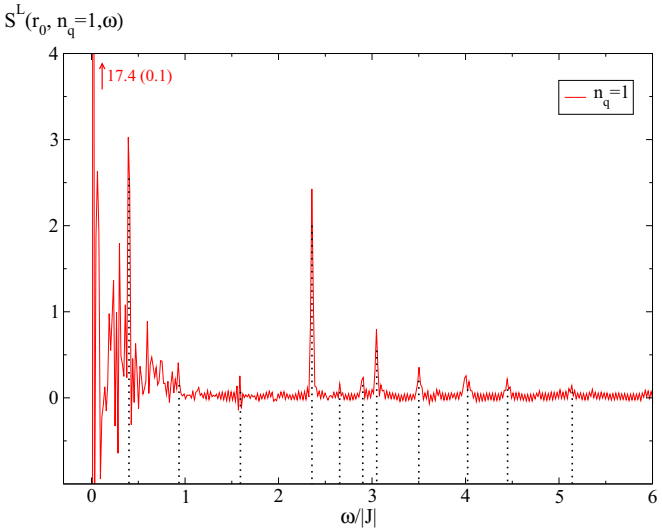

FIG. 7. (Color online) The spectra for $S^L(\mathbf{r}_0,\mathbf{q},\omega)$ obtained from isotropic, antiferromagnetic nanofilm with a lattice size of $L_{xy} = L_z = 20$. The results were obtained in the *PBCXY* [100] directions, i.e., the directions parallel to the free surfaces, with $\mathbf{r}_0 \Rightarrow$ bulk center at $T = 0.4T_N$ with SD parameters of $n_t = 5000$, $n_{\text{cutoff}} = 4000$, and $dt = 0.2/|J|$. We give the spectra for the wave vector of $n_q = 1$. The excitation peaks labeled with thin black dashed lines are the peaks "contaminated" by the transverse component of the local multiple spin-wave excitations shown in Fig. 6.

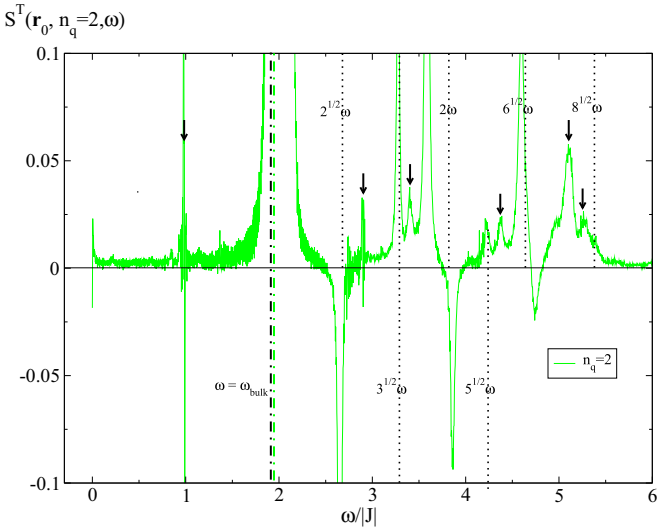

FIG. 8. (Color online) Determination of multiple spin-wave excitation locations with the assumption of q-space spin-wave reflection with broken momentum conservation in the linear dispersion region with small momentum of $n_q = 2$ for an isotropic, antiferromagnetic nanofilm with a lattice size of $L_{xy} = L_z = 20$. The results were obtained in the *PBCXY* [100] directions, i.e., the directions parallel to the free surfaces, with $\mathbf{r}_0 \Rightarrow$ bulk center at $T = 0.4T_N$ with SD parameters of $n_t = 5000$, $n_{\text{cutoff}} = 4000$, and $dt = 0.2/|J|$. The thick green dashed line gives the single spin-wave excitation location for the wave vector of $n_q = 2$ of the system with periodic boundary conditions; the thick black dashed line labeled with $\omega = \omega_{\text{bulk}}$ gives the bulk excitation location for the wave vector of $n_q = 2$ of the nanofilm; the thick black downward arrows labeled in figure give the locations of excitation peaks disturbed by the unexpected excitation modes in *FBCZ* [100] perpendicular directions that will be discussed in Sec. III E.

of the nanofilm. To locate multiple spin-wave excitation locations quantitatively, we took the bulk energy frequency $\omega = \omega_{\text{bulk}}$ and then multiplied it with all possible ratios of $\frac{q_{\text{refl}}}{q_{\text{bulk}}}$, which are illustrated in Fig. 5. The results of those multiplications are shown by thin black dashed lines with a ratio multiplying ω labeled on each. The thick black downward arrows labeled in Fig. 6 give the locations of excitation peaks disturbed by the unexpected excitation modes in *FBCZ* [100] perpendicular directions that will be discussed in Sec. III E.

For completeness, in Fig. 7 we show the spectra for the longitudinal component of the local dynamic structure factor, i.e., $S^L(\mathbf{r}_0,\mathbf{q},\omega)$, for isotropic, antiferromagnetic nanofilm with the same lattice size, i.e., $L_{xy} = L_z = 20$. We labeled the y axis of our results with $S^L(\mathbf{r}_0,n_q,\omega)$ for the wave vector of $n_q = 1$. The excitation peaks labeled with thin black dashed lines are the peaks "contaminated" by the transverse component of the local multiple spin-wave excitations shown in Fig. 6. Note that the "contamination" of the spin-wave excitations is caused by imperfect regrouping of longitudinal and transverse components of spin-wave excitations to the antiferromagnetic order parameter, as we discussed in Sec. II C.

Similarly, Fig. 8 shows that the multiple spin-wave excitation locations with $n_q = 2$ are also determined quantitatively.

Comparing the results in Figs. 6 and 8, we observed that, with our assumption of q-space spin-wave reflection, the proportion of successfully explained multiple excitations with $n_q = 1$ is larger than that with $n_q = 2$, which means our assumption works better with $n_q = 1$ than $n_q = 2$, i.e., it works better with a smaller momentum. This is reasonable considering that the linear dispersion region with small momentum q is the region for the assumption to be correctly applied.

C. Spectra for $S^T(\mathbf{r}_0,\mathbf{q},\omega)$ for isotropic antiferromagnetic nanoparticles

In this section, we give the results for the transverse component of the local dynamic structure factor $S^T(\mathbf{r}_0,\mathbf{q},\omega)$ with $\mathbf{r}_0 \Rightarrow$ bulk center for isotropic, antiferromagnetic nanoparticles on an $L \times L \times L$ simple-cubic lattice. The results were obtained in six symmetric [100] directions, as shown in Fig. 9.

Figure 10 shows the spectra for $S^T(\mathbf{r}_0,\mathbf{q},\omega)$, obtained from isotropic, antiferromagnetic nanoparticles with $L = 10$, 14, and 20. For convenience of labeling, we labeled the y axis of our results with $S^T(\mathbf{r}_0,n_q,\omega)$ with $n_q = 0,1,2,\ldots$ [defined in Eq. (4)]. In the figure, we give the spectra for $S^T(\mathbf{r}_0,n_q,\omega)$ with $n_q = 1,2,\ldots,5$.

Multiple excitation peaks for wave vectors within the first Brillouin zone appear in the spin-wave spectra for the transverse component of the local dynamic structure factor $S^T(\mathbf{r}_0,n_q,\omega)$ in the classical Heisenberg isotropic antiferromagnetic nanoparticles, which are lacking if periodic boundary conditions are used.

As noted previously, the bigger oscillations of the spectra for $n_q = 1$ in Fig. 10 for $L = 20$ are due to the finite-time cutoff n_{cutoff}, which introduces oscillations, can be smoothed out by convoluting the local correlation function with a Gaussian resolution function in the time Fourier transformation.

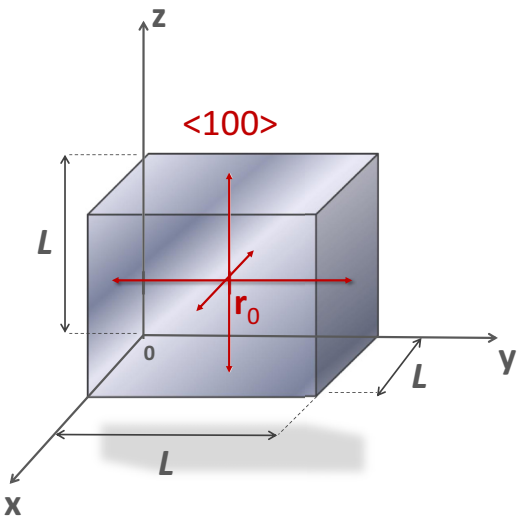

FIG. 9. (Color online) [100] directions with $\mathbf{r}_0 \Rightarrow$ bulk center for isotropic, antiferromagnetic nanoparticles.

The shifting to lower energy frequency of the main excitation peak in the figure is due to the finite-size effects.

D. Quantitative explanation of multiple spin-wave excitations in the spectra for $S^T(\mathbf{r}_0,\mathbf{q},\omega)$ for isotropic antiferromagnetic nanoparticles with the assumption of q-space spin-wave reflection

As shown in Fig. 10, the spectra for isotropic, antiferromagnetic nanoparticles are even more complicated than the spectra for isotropic, antiferromagnetic nanofilms given in Figs. 2 and 3. Not only are there many more multiple spin-wave excitations for each wave vector, but also the

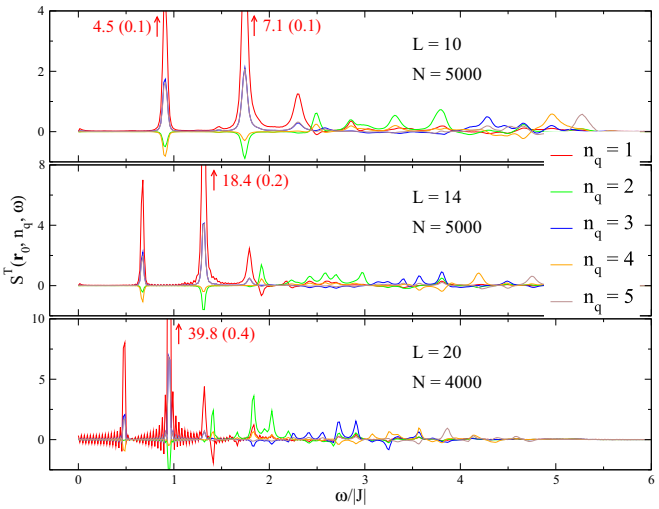

FIG. 10. (Color online) The spectra for $S^T(\mathbf{r}_0,\mathbf{q},\omega)$ obtained from isotropic, antiferromagnetic nanoparticles with $L = 10$, 14, and 20. The results were obtained in the [100] directions with $\mathbf{r}_0 \Rightarrow$ bulk center at $T = 0.4T_N$ with SD parameters of $n_t = 5000$, $n_{\text{cutoff}} = 4000$, and $dt = 0.2/|J|$. We give the spectra for $n_q = 1,2,\ldots,5$.

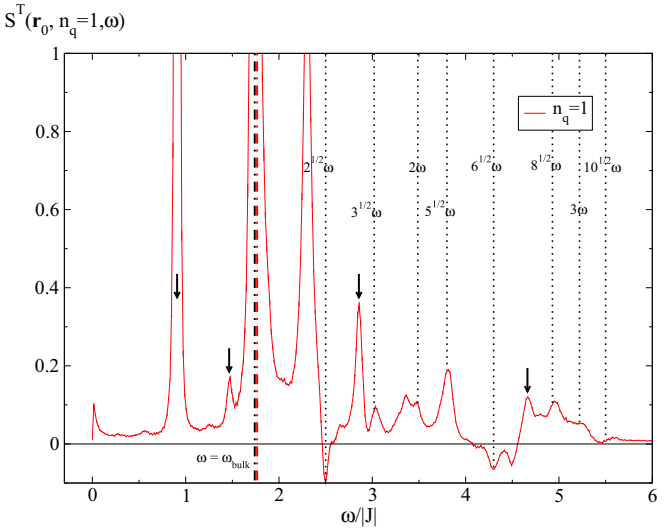

FIG. 11. (Color online) Determination of multiple spin-wave excitation locations with the assumption of q-space spin-wave reflection with broken momentum conservation in the linear dispersion region with small momentum of $n_q = 1$ for an isotropic, antiferromagnetic nanoparticle with a lattice size of $L = 10$. The results were obtained in the [100] directions with $\mathbf{r}_0 \Rightarrow$ bulk center at $T = 0.4T_N$ with SD parameters of $n_t = 5000$, $n_{\text{cutoff}} = 4000$, and $dt = 0.2/|J|$. The thick red dashed line gives the single spin-wave excitation location for the wave vector of $n_q = 1$ of the system with periodic boundary conditions; the thick black dashed line labeled with $\omega = \omega_{\text{bulk}}$ gives the bulk excitation location for the wave vector of $n_q = 1$ of the nanoparticle; the thick black downward arrows labeled in the figure give the locations of excitation peaks disturbed by the unexpected excitation modes in *FBCZ* [100] perpendicular directions that will be discussed in Sec. III E.

excitation patterns themselves become more intricate. Those observations are due to the fact that the completely laterally confined nanoparticles have much stronger free-surface effects on the dynamics than those of nanofilms. However, in the linear dispersion region with the assumption of q-space spin-wave reflection, we can still determine the locations of those excitations quantitatively.

Figure 11 gives the spectra for $n_q = 1$ of the nanoparticle with a lattice size of $L = 10$. The thick red dashed line gives the single spin-wave excitation location for the wave vector of $n_q = 1$ of the system with periodic boundary conditions; the thick black dashed line labeled with $\omega = \omega_{\text{bulk}}$ gives the bulk excitation location for the wave vector of $n_q = 1$ of the nanoparticle; the determination of multiple spin-wave excitation locations is shown by thin black dashed lines with a ratio multiplying ω labeled on each; the thick black downward arrows labeled in the figure give the locations of excitation peaks disturbed by the unexpected excitation modes in *FBCZ* [100] perpendicular directions, to be discussed in Sec. III E.

E. Observation of two unexpected quantized spin-wave excitation modes for $S^T(\mathbf{r}_0,\mathbf{q},\omega)$ for isotropic antiferromagnetic nanofilms

In this section, we give the results for the transverse component of the local dynamic structure factor $S^T(\mathbf{r}_0,\mathbf{q},\omega)$ with

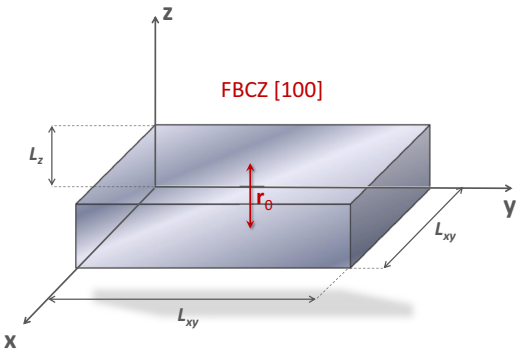

FIG. 12. (Color online) *FBCZ* [100] directions with $\mathbf{r}_0 \Rightarrow$ bulk center for isotropic, antiferromagnetic nanofilms.

$\mathbf{r}_0 \Rightarrow$ bulk center for isotropic, antiferromagnetic nanofilms on an $L_{xy} \times L_{xy} \times L_z$ simple-cubic lattice. The results were obtained in the free boundary directions, denoted as the *FBCZ* [100] directions, perpendicular to the free surfaces, as shown in Fig. 12.

Figure 13 shows the spectra for $S^T(\mathbf{r}_0,\mathbf{q},\omega)$ with $L_{xy} = L_z = 20$. In the figure, we give the spectra for $n_q = 0,1,2,\ldots,4$. As shown in the figure, we observed two unexpected quantized spin-wave excitation modes for $S^T(\mathbf{r}_0,n_q,\omega)$, i.e., "Excitation Mode I" and "Excitation Mode II," in the spatial z direction in isotropic, antiferromagnetic nanofilms. This unexpected form of spin-wave excitation behavior needs further study, but at least our results indicate that those unexpected quantized excitation modes could be potentially caused by, but are not limited to, the free-surface confinement effects.

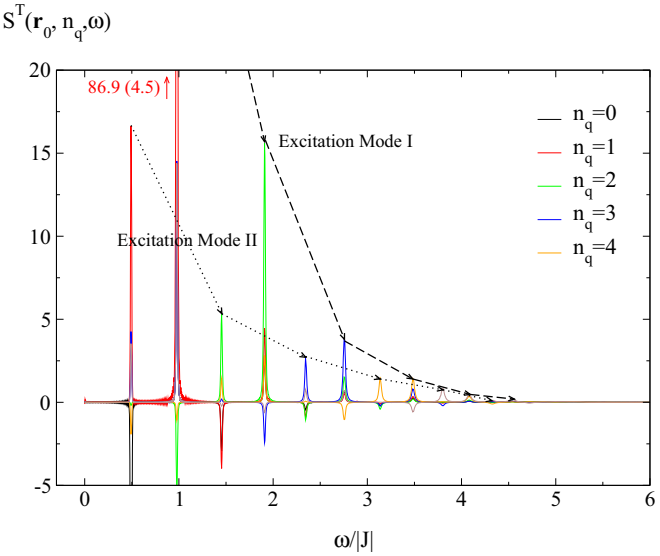

FIG. 13. (Color online) The spectra for $S^T(\mathbf{r}_0,\mathbf{q},\omega)$ obtained from isotropic, antiferromagnetic nanofilms with $L_{xy} = L_z = 20$. The results were obtained in the *FBCZ* [100] directions, i.e., the directions perpendicular to the free surfaces, with $\mathbf{r}_0 \Rightarrow$ bulk center at $T = 0.4T_N$ with SD parameters of $n_t = 5000$, $n_{\text{cutoff}} = 4000$, and $dt = 0.2/|J|$. We give the spectra for $n_q = 0,1,2,\ldots,4$. N is the total number of initial configurations.

IV. CONCLUSION

With large-scale Monte Carlo and spin dynamics simulations, we have investigated the dynamic behavior of antiferromagnetic nanostructures on a simple-cubic lattice geometry, using an isotropic, classical Heisenberg model of classical spins with unit length and with the nearest-neighbor exchange interactions. Nanoparticles are modeled with completely free boundary conditions, and nanofilms are modeled with partially free boundary conditions, i.e., two free surfaces in the spatial z direction and periodic boundaries parallel to the surfaces in the x and y directions. Hybrid Monte Carlo methods are used to obtain the static properties of modeled nanostructures. The Monte Carlo methods are also used to generate equilibrium spin configurations as initial states of the coupled differential equations of motion. A fast spin dynamics algorithm based on the fourth-order Suzuki-Trotter decomposition of exponential operators has been applied to integrate the equations of motion. Our spin dynamics simulations are performed at a low temperature $T = 0.4T_N$. The integrations are carried to $n_{\text{cutoff}} = 4000$ with an SD time step $dt = 0.2/|J|$.

With the time evolution of the spin configurations, the local space- and time-displaced spin-spin correlation function $C(\mathbf{r}_0,\mathbf{r},t)$ is calculated, where $\mathbf{r}_0$ denotes the starting point from which the correlation function is calculated and can be chosen to be fixed at the bulk center or the surface center of nanoparticles and nanofilms, or the lattice corner of nanoparticles in the simulations. The local dynamic structure factor $S(\mathbf{r}_0,\mathbf{q},\omega)$ is the Fourier transformation of $C(\mathbf{r}_0,\mathbf{r},t)$, which can be observed in inelastic magnetic neutron scattering. For the temperature $T = 0.4T_N$, compared to the single spin-wave excitation spectra for the "infinite" system with fully periodic boundary conditions, much more complicated excitation spectra for the transverse component of the local dynamic structure factor $S^T(\mathbf{r}_0,\mathbf{q},\omega)$ appear in the nanoscale classical Heisenberg antiferromagnets. The spectra for $S^T(\mathbf{r}_0,\mathbf{q},\omega)$ have multiple excitation peaks for wave vectors within the first Brillouin zone, which are lacking if periodic boundary conditions are used. We were able to simulate these systems with sufficiently high accuracy such that multiple excitation peaks distinguish themselves from the intrinsic simulation noise by showing a significant difference in magnitude between the two signals. With the assumption of q-space spin-wave reflection with broken momentum conservation due to lateral free-surface confinements, we successfully explained the locations of those excitations quantitatively for isotropic, antiferromagnetic nanostructures in the linear dispersion region with small wave vectors.

The results of this study indicate the presence of unexpected forms of spin-wave excitation behavior that have yet to be observed experimentally but could be directly tested through neutron scattering experiments on nanoscale $RbMnF_3$ films or particles.

ACKNOWLEDGMENTS

We are indebted to S.-H. Tsai for very helpful discussions and for assistance on computing techniques. We would also like to thank X. Tao and J. Yin for valuable discussions.

Computer simulations were carried out on the ORNL Institutional Cluster (OIC) at Oak Ridge National Laboratory, and the IBM Cluster (pcluster) at the University of Georgia. This research was supported in part by UT-Battelle Subcontract No. 4000040811, and the Office of Basic Energy Sciences, Materials Sciences and Engineering Division.

[1] A. Tucciarone, H. Y. Lau, L. M. Corliss, A. Delapalme, and J. M. Hastings, Phys. Rev. B **4**, 3206 (1971).
[2] U. J. Cox, R. A. Cowley, S. Bates, and L. D. Cussen, J. Phys. Condens. Matter **1**, 3031 (1989).
[3] R. Coldea, R. A. Cowley, T. G. Perring, D. F. McMorrow, and B. Roessli, Phys. Rev. B **57**, 5281 (1998).
[4] K. Chen and D. P. Landau, Phys. Rev. B **49**, 3266 (1994).
[5] A. Bunker, K. Chen, and D. P. Landau, Phys. Rev. B **54**, 9259 (1996).
[6] S.-H. Tsai, A. Bunker, and D. P. Landau, Phys. Rev. B **61**, 333 (2000).
[7] S.-H. Tsai, A. Bunker, and D. P. Landau, Comput. Phys. Commum. **147**, 1 (2002).
[8] S.-H. Tsai and D. P. Landau, Phys. Rev. B **67**, 104411 (2003).
[9] X. Tao, D. P. Landau, T. C. Schulthess, and G. M. Stocks, Phys. Rev. Lett. **95**, 087207 (2005).
[10] G. F. Mazenko, M. J. Nolan, and R. Freedman, Phys. Rev. B **18**, 2281 (1978).
[11] R. Freedman and G. F. Mazenko, Phys. Rev. Lett. **34**, 1575 (1975); Phys. Rev. B **13**, 4967 (1976).
[12] A. Cuccoli, S. W. Lovesey, and V. Tognetti, J. Phys.: Condens. Matter **6**, 7553 (1994).
[13] P. C. Hohenberg and B. I. Halperin, Rev. Mod. Phys. **49**, 435 (1977).
[14] B. I. Halperin and P. C. Hohenberg, Phys. Rev. **177**, 952 (1969).
[15] A. Bunker and D. P. Landau, Phys. Rev. Lett. **85**, 2601 (2000).
[16] B. Hillebrands and K. Ounadjela, in *Spin Wave Confinement*, edited by S. O. Demokritov (Pan Stanford, Singapore, 2009), p. 38.
[17] C. Mathieu, J. Jorzick, A. Frank, S. O. Demokritov, A. N. Slavin, B. Hillebrands, B. Bartenlian, C. Chappert, D. Decanini, F. Rousseaux, and E. Cambril, Phys. Rev. Lett. **81**, 3968 (1998).
[18] J. Jorzick, C. Krämer, S. O. Demokritov, B. Hillebrands, B. Bartenlian, C. Chappert, D. Decanini, F. Rousseaux, E. Cambril, E. Søndergard, M. Bailleul, C. Fermon, and A. N. Slavin, J. Appl. Phys. **89**, 7091 (2001).
[19] M. Kostylev, V. E. Demidov, U.-H. Hansen, and S. O. Demokritov, Phys. Rev. B **76**, 224414 (2007).
[20] J. Jorzick, S. O. Demokritov, C. Mathieu, B. Hillebrands, B. Bartenlian, C. Chappert, F. Rousseaux, and A. N. Slavin, Phys. Rev. B **60**, 15194 (1999).
[21] G. Brown, A. Janotti, M. Eisenbach, and G. M. Stocks, Phys. Rev. B **72**, 140405 (2005).
[22] G. Brown, J. Appl. Phys. **103**, 07D504 (2008).
[23] R. W. Gerling and D. P. Landau, Phys. Rev. B **41**, 7139 (1990).
[24] D. P. Landau and M. Krech, J. Phys.: Condens. Matter **11**, R179 (1999).
[25] M. Creutz, Phys. Rev. D **36**, 515 (1987).
[26] F. R. Brown and T. J. Woch, Phys. Rev. Lett. **58**, 2394 (1987).
[27] M. Krech, A. Bunker, and D. P. Landau, Comput. Phys. Commun. **111**, 1 (1998).
[28] D. P. Landau, A. Bunker, H. G. Evertz, M. Krech, and S.-H. Tsai, Prog. Theor. Phys. Suppl. **138**, 423 (2000).